

Calculation and Accurate Measurement of Capacitance of Electrically Small Axi-symmetric Microstructures near a Probe Tip

Tao Zhang[^] and M. Tabib-Azar^{^*}

^{^*} Electrical Engineering and Computer Science Department

^{*} Macromolecular Science & Physics Departments

Case Western Reserve University

Cleveland, OH

ABSTRACT -An efficient calculation method that uses semi closed-form solutions of axi-symmetric metallic sub-sections to numerically calculate the capacitance of a metallic probe over stratified dielectric substrates or metallic samples is developed and discussed. The current continuity equation was first used to obtain charge densities at the structure's surface. The capacitance matrix that uses gap and permittivity (CGP) as indexes for specific tip was then numerically estimated using this method. CGP matrix enabled non-contact simultaneous topography and permittivity mapping using a single microwave measurement. This method was subsequently used to calculate the capacitance of spherical and conical tips commonly used in local scanning probe microscopy. To evaluate the accuracy of the this method, the load impedance change of the above structures were measured and compared to their numerical values. The load impedance of the probe tip was experimentally determined from the input impedance of a $\lambda/2$ microstrip resonator at 1 GHz. The model of the measurement apparatus and a calibration procedure were also developed. The experimental data agreed with the numerical results quite well. Moreover, the experiments also showed that the simple $\lambda/2$ microstrip resonator has an excellent capacitance resolution nearing 1.96×10^{-18} F at 1 GHz using a BiCMOS I/Q detector.

I. INTRODUCTION

The axi-symmetric, electrically small structures are important in many applications. For example, the electrically short monopole antenna for Loran-C reception [1] is a truncated cone where charge density analysis is used to optimize effective height of antenna. Metallic cylinders and truncated cones are also widely used as antenna in orbital satellites.

Another interesting example is the probes that are used in local probe microscopy. The conductive atomic force microscope (c-AFM) or its close relative the evanescent microwave probe (EMP) [2-10] and the scanning capacitance microscope (SCM) probes all have conical or spherical shapes that along with the sample form a capacitor structure with very small but detectable capacitance or impedance at a given operation frequency. More precisely, the load impedance near the tip depends on the sample's morphology, electrical property and tip structure. Imaginary part of this impedance is the gap capacitor between the metallic tip and semiconductor or insulator sample. The sheet resistance of the sample determines the real part of this impedance. To increase the lateral spatial resolution of the EMP, c-AFM and SCM, the tip-

sample impedance should be optimized to yield smallest possible fringing fields and largest response to tip-sample interaction.

The MOS capacitance of the tip-oxide-semiconductor structure encountered in SCM measurements has been a subject of intense investigations by many groups. In the present work a semi-closed form capacitance calculation method for axi-symmetric structures over stratified dielectrics or metal was developed and compared with the experimental results. This fast calculation method can be used to a) compile a look-up table for capacitance values for calibration, b) estimate stand-off distance during non-contact imaging process and c) estimate the electromagnetic field or charge distribution at in the sample.

A microwave resonator terminated by a tip is very sensitive to the impedance changes near the tip [2,3]. In order to quantitatively obtain the real and imaginary parts of the load impedance, an accurate model of resonator is needed. The past efforts used discrete components to model the transmission line. Few of these models were able to extract impedance near the probe tip. In this paper an accurate model of the microstrip line resonator and corresponding calibration procedure have been developed. The extracted impedance change near the resonant frequency agrees with the calculated impedance quite well.

We prefer using the load impedance near the tip Z_l for the quantitative imaging process instead of using resonant frequency shift Δf , or the quality factor (Q) or the magnitude of the AM demodulation because of the following advantages.

- 1) Z_l can be compared with numerical results directly and simulated to optimize the measurement system.
- 2) Z_l is obtained using fast single frequency measurement. Ultra-stable and low-cost dielectric oscillator can be used as signal source. Δf and Q-factor are property of frequency spectrum. Complicated phase lock-loop circuits may be needed to track Δf which limits the measurement speed and accuracy. Using FM modulation and demodulation to measure the Q-factor needs an additional calibration step and may not be accurate.
- 3) The experimental determination of Z_l is self-corrected. Z_l should be almost the same using different measurement frequencies. In contrast, the input impedance changes drastically near the resonant frequency.
- 4) Z_l is independent of measurement system and carrier frequency. Δf , Q-factor and magnitude of AM demodulation signal depend on measurement system and carrier frequency.

In the following sections we show how Z_l is calculated and extracted from the resonator measurements. In the next section, we will discuss the calculation method followed by the measurement procedure and analysis.

II. CAPACITANCE OF METALLIC TIPS

Axi-symmetric surfaces are the sum of curved surfaces and flat surfaces that are partitioned to subsections as shown in figure 1.

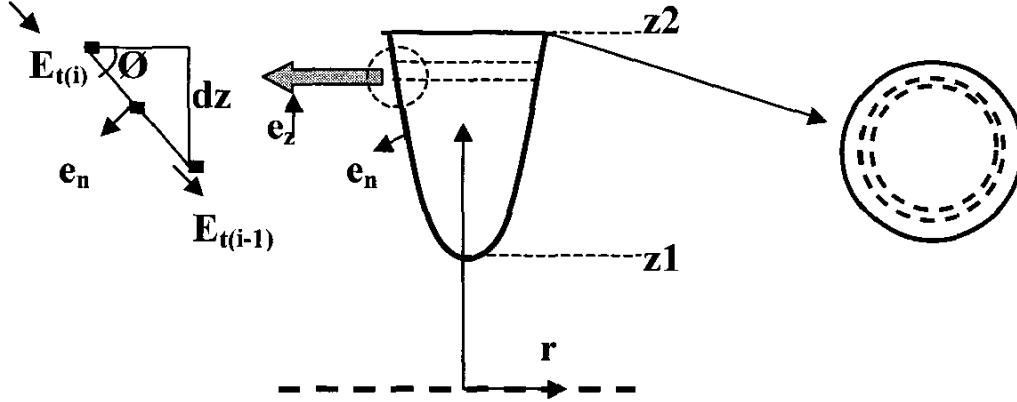


Figure 1 Axi-symmetric surface is the sum of curved surfaces and flat surfaces. Axi-symmetric subsections are divided.

We assume charge Q_i ($1 \leq i \leq N$) is at the center of the subsection "i" and the total charge is constant Q ($\sum_{i=1}^N Q_i$). This assumption is the same as the Monte Carlo minimization method [11].

But we update the Q_i using tangent electrical field E_t at the interfaces between subsection "i" and subsection "i+1" instead of stochastically generating numbers. At $n+1^{\text{th}}$ iteration, we get:

$$Q_i^{n+1} = Q_i^n - \epsilon_0 E_{t(i-1)}^n l_{i-1} \quad (1a)$$

$$Q_i^{n+1} = Q_i^n + \epsilon_0 E_{t(i)}^n l_i \quad (1b)$$

where ϵ_0 is permittivity, l_i is the length of i^{th} interface and $\epsilon_0 E_{t(i)}^n l_i$ is virtual current because of non-equilibrium charge distribution. The iterations keep Q constant for isolated conductors. The physical background of this algorithm (dynamics) makes convergence assured.

The above iteration process converges much faster than stochastic method. Instead of using this improved iteration method ($O(N^2)$) we use GMRES ($O(N)$) to solve the linear equation.

$$\begin{bmatrix} [k(i, j)]_{(N-1) \times N} \\ [1]_{1 \times N} \end{bmatrix} \begin{bmatrix} Q_j \end{bmatrix}_{N \times 1} = \begin{bmatrix} [0]_{(N-1) \times 1} \\ Q \end{bmatrix} \quad (2)$$

The tangent electrical field $E_t(i, j)$ at i^{th} interface because of charge in j^{th} subsection is

$$E_t(i, j) = k(i, j) * Q_j = [E_z(i, j) \cos \phi - E_r(i, j) \sin \phi] \quad (3)$$

$E_z(i, j)$ and $E_r(i, j)$ are the axial-field component and the radial-field component of i^{th} section because of j^{th} charge and its image charge respectively:

$$\begin{aligned} E_z(i, j) &= E_z(r_i, z_j) - E_z(r_i, -z_j) \\ E_r(i, j) &= E_r(r_i, z_j) - E_r(r_i, -z_j) \end{aligned} \quad (4)$$

where

$$\begin{aligned}
E_z(r_i, z_j) &= \frac{Q_j}{4\pi\epsilon_0} \frac{(z_i - z_j)E(k)}{2\pi((r_i - r_j)^2 + (z_i - z_j)^2)\sqrt{((r_i + r_j)^2 + (z_i - z_j)^2)}} \\
E_r(r_i, z_j) &= \frac{Q_j}{4\pi\epsilon_0} \frac{((r_i - r_j)^2 + (z_i - z_j)^2)K(k) - (-r_i^2 + r_j^2 + (z_i - z_j)^2)E(k)}{2\pi r_i((r_i - r_j)^2 + (z_i - z_j)^2)\sqrt{((r_i + r_j)^2 + (z_i - z_j)^2)}}
\end{aligned} \quad (5)$$

where K and E are complete elliptic integrals of the first kind and second kind respectively, k is

$$k = \frac{2\sqrt{r_i r_j}}{\sqrt{((r_i + r_j)^2 + (z_i - z_j)^2)}} \quad (6)$$

Capacitance C can be obtained from charge distribution $[Q_j]_{N \times 1}$:

$$C = \frac{Q}{V^i} \quad (7)$$

where,

$$V^i = \sum_{j=1}^{N-1} \frac{Q_j}{4\pi\epsilon_0} \frac{4r_j K(k)}{2\pi r_j \sqrt{((r_i + r_j)^2 + (z_i - z_j)^2)}} \quad (8)$$

This iteration process is easily expanded to axi-symmetric probe above multiple stratified dielectric samples.

For tip over dielectric sample with thickness h, the charge density $\rho(z)$ is the solution to the integral equation

$$\rho(z) = \int_{z_j} \frac{1}{4\pi\epsilon_0} \frac{\rho(z_j)}{2\pi r_j} \frac{4r_j K(k)}{\sqrt{(r+r_j)^2 + (z-z_j)^2}} dz + \sum_{i=1}^{\infty} \int_{z_i'} \frac{1}{4\pi\epsilon_0} \frac{\rho_i(z_i')}{2\pi r_i} \frac{4r_i K(k')}{\sqrt{(r+r_i)^2 + (z-z_i')^2}} dz \quad (9)$$

where z_i' is given by

$$\begin{aligned}
z_{11}' &= -z - 2h_i \\
z_{ii}' &= -z - 2h_i - 2(i-1)h,
\end{aligned} \quad (10)$$

where h_i is z coordinate of lth charge on the tip surface when the origin of z axis is at sample surface.

The ith image charge of lth charge on the tip surface is $\rho_i(z_{ii}') = \gamma_i \rho(z_i)$. The scalar factor γ_i is given by

$$\begin{aligned}
\gamma_1 &= \frac{\epsilon_0 - \epsilon_1}{\epsilon_0 + \epsilon_1} \\
\gamma_i &= -\left(\frac{\epsilon_0 - \epsilon_1}{\epsilon_0 + \epsilon_1}\right)^i \frac{2\epsilon_0}{\epsilon_0 + \epsilon_1} \frac{2\epsilon_1}{\epsilon_0 + \epsilon_1}
\end{aligned} \quad (11)$$

where ϵ_1 is dielectric constant of underneath dielectric sample.

The integration equation again is solved by solving 'current' equation (2) on the probe surface using the charges in the tip and image charges in the sample. $E_z(i, j)$ and $E_r(i, j)$ change to:

$$E_z(i, j) = E_z(r_i, z_j) + \gamma_i \sum_{i=1}^{\infty} E_z(r_i, z_{ii}') \quad (12)$$

$$E_r(i, j) = E_r(r_i, z_j) + \gamma_i \sum_{i=1}^{\infty} E_r(r_i, z_{ii}')$$

If the radius of the probe tip is small compared to sample thickness, computation using only 1st image charge and charge in the tip gives a good approximation.

III. ACCURATE MEASUREMENT OF LOAD IMPEDANCE

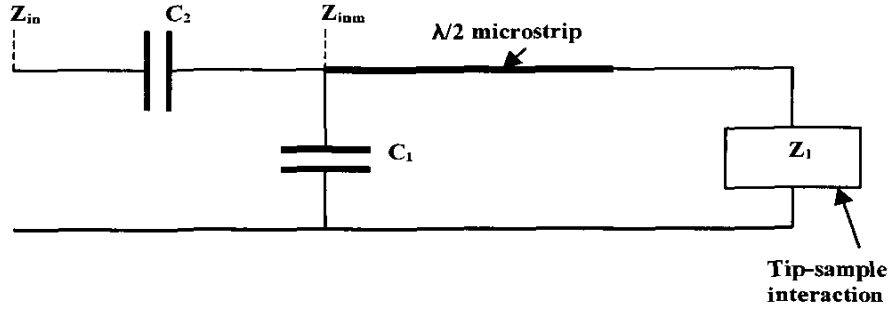


Figure 2 Simplified model of gap capacitor, $\lambda/2$ microstrip line and load impedance near the probe tip because of tip-sample interaction.

We used evanescent microwave probes developed in our group during the past 12 years [3-5]. These microstrip line based system have sub-micron spatial resolution and various applications [6-10]. The final simplified model of our measurement system using $\lambda/2$ microstrip line is shown in figure 2. The input impedance including the gap capacitor is

$$Z_m = \frac{Z_{inm}}{j\omega C_1 Z_{inm} + 1} + \frac{1}{j\omega C_2} \quad (13)$$

We also have developed a transmission equation that relates Z_{inm} with load impedance Z_1 near the probe tip. The calibration procedure using this model is carefully designed and all the parameters are experimentally determined. The reference plane of the input impedance is carefully calibrated. The load impedance near the probe tip then can be accurately determined by measuring the input impedance before the gap capacitor.

Capacitance Measurements. One extraction process near resonant frequency is shown in figure 3a (extracted load impedance at the tip) and figure 3b (measured input impedance Z_{in}) from 995 MHz to 1000 MHz using vector measurement system. The extracted C_1 was 2.99×10^{-13} F and

C_2 was 3.3979×10^{-13} F at 996 MHz. The change in the tip impedance (figure 3a) was very small while the input impedance change (figure 3b) was very large. The figure 3b clearly shows a nearly open condition that is expected. These observations show that the model in section III is quite good for load impedance extraction.

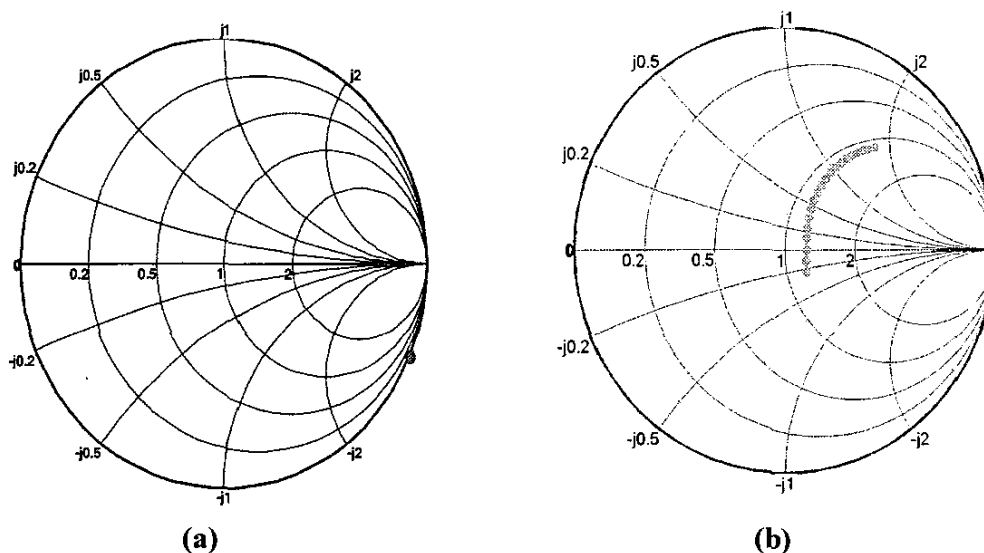


Figure 3 Extracted load impedance (a) at the tip from input impedance (b) from is nearly open which is expected. The frequency is from 995 MHz to 1000 MHz.

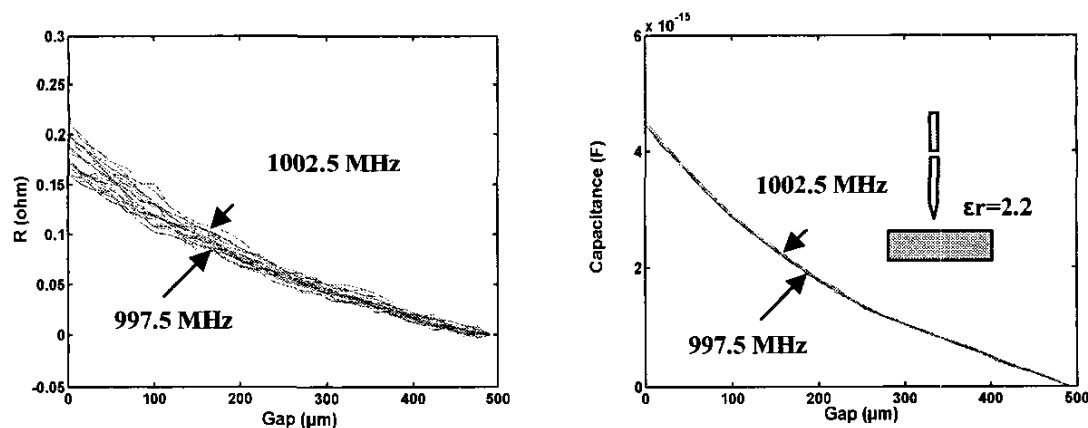


Figure 4 Extracted convergent capacitance and resistance change at the tip of a microstrip resonator versus different gap.

The extraction was convergent or self-corrected near resonant frequency. Figure 4 shows extracted capacitance and resistance near the tip of a microstrip resonator with different air gaps. The resonant frequency of the resonator was 1 GHz and 20 equally-spaced frequencies in 5 MHz bandwidth near resonant frequency was used. The convergence of capacitance was better than

the convergence of the resistance change. The nearly identical results imply that the extraction was robust and stable with respect to noise and frequency shift. Reliable impedance estimation can be obtained by averaging over values obtained at multiple frequencies. Figure 5 shows corresponding magnitude versus gap measured using the I-Q mixer near the probe's resonant frequency. The swing of the magnitude was ultra sensitive to the frequency. Small shift of circuit parameters and operation frequency affected the output signal drastically.

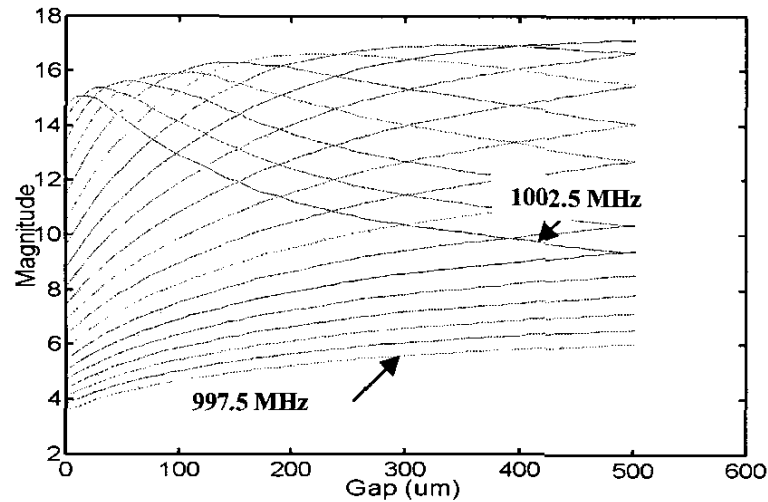


Figure 5 Corresponding S11s (Magnitude) near resonant frequency were not convergent.

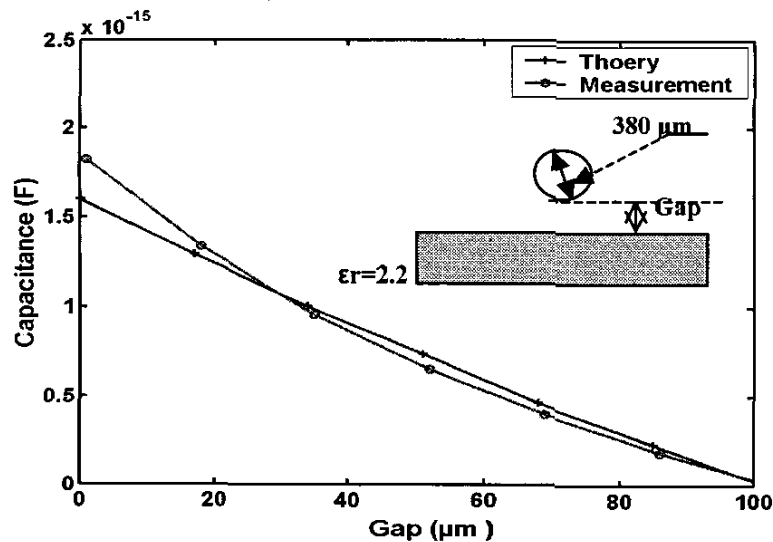


Figure 6 Measured and calculated capacitance change of the spherical tip with 380 μm diameter as a function of tip-sample stand-off distance at 1 GHz.

Figure 6 shows the capacitance change versus gap between 380 μm ball bearing (<5% tolerance) and 0.785 mm thick Duroid substrate (dielectric constant=2.2). The measurement result agrees with the calculated capacitance quite well. In this experiment the resonator was

tuned to have smallest possible return loss and hence maximum loaded quality factor in free space near 1 GHz. The input impedance was measured using a network analyzer with 20MHz frequency span and frequency resolution of 100 KHz. The insertion loss of the resonator was 40dB at f_0 and Q factor was around 100 in free space. A copper sphere was attached to the tip during characterization because it has a well-defined geometry.

For the spherical tip, the load impedance changed from $52.9096 + 3.1801i$ near the surface to $53.6537 + 4.8995i$ at $108 \mu\text{m}$ stand-off distance. To estimate the sensitivity of the $\lambda/2$ resonator, we used a BiCMOS vector measurement system. The measurement frequency was fixed at the resonant frequency of the probe in free space. As the probe-sample distance changed from $108 \mu\text{m}$ to $1 \mu\text{m}$, the magnitude of the reflected signal changed by 44.5 mV and phase changed by 48.1 mV. The capacitance change over the $108 \mu\text{m}$ stand-off variation was measured using the BiCMOS based vector measurement system to be $+1.88 \times 10^{-15}$ F. Thus, the average sensitivity of this $\lambda/2$ resonators was 3.91×10^{-17} F/mV using phase signal. Therefore, for a typical noise level of 0.05 mV of BiCMOS system, the capacitance resolution was 1.96×10^{-18} F. Lower noise GaAs HEMT device measurement system and better temperature control can be used to further improve the probe's sensitivity.

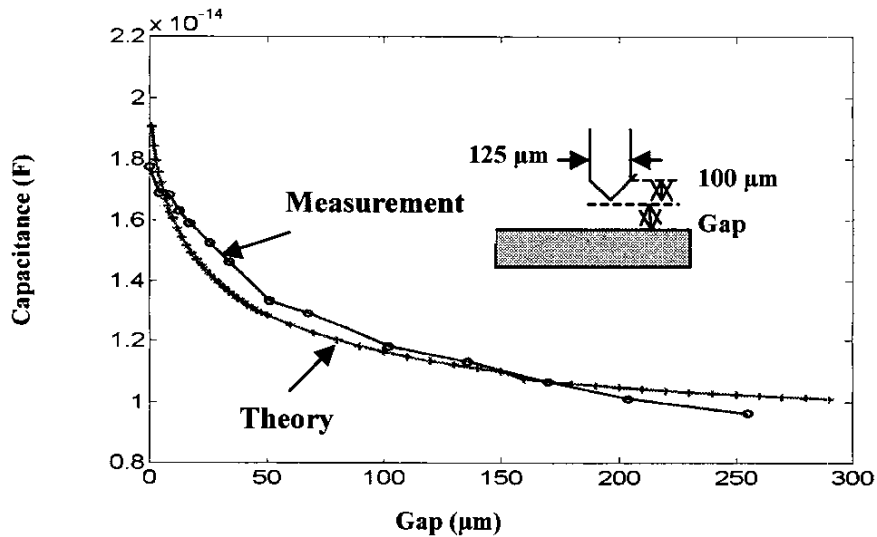


Figure7 Measured capacitance of spherical and conical (Ti) tips as a function of tip-sample stand-off distance at 1 GHz.

Scanning tunneling microscope (STM) based measurements use atomically sharp tungsten tips. Such a tip was characterized using the above method. Figure 7 shows the calculated and measured capacitance of an atomically sharp tungsten tip as a function of the tip-sample stand-off distance at 1 GHz. The tip geometry is depicted in the inset.

Permittivity Measurements. Non-contact permittivity measurement is important for characterizing ultra-clean or delicate samples. The efficient numerical method discussed in this paper is used to estimate gap and permittivity at the same time. The capacitance change matrix (CGP) that uses gap and permittivity as indexes for specific tip is numerically estimated using

algorithm discussed in section II. From CGP, the permittivity matrix (PCC) and the topography matrix (TCC) can be estimated. TCC uses capacitance at gap g_1 and gap g_2 ($g_2=g_1-d$, d is constant). Because the indexes C_{g_1} and C_{g_2} are both monotonic function of gap, two-dimensional data interpolation algorithm can be used to determine the permittivity and gap. Accurate determination of probe size or a z-decay measurement above metallic ground is the only calibration step that is need in this method.

In the above technique, the capacitance changes at gap g_1 and gap g_2 were experimentally extracted and used as indexes of PCC and TCC. The step of the gap used to generate the matrixes was $8.5 \mu\text{m}$, d was $17 \mu\text{m}$ and the dielectric constant step was 0.2 from 2-12 in our experiment. The measured permittivity versus the value from the manufactures was plotted in figure 8. Less than 7% difference between measured permittivity and value provided by manufactures has been achieved.

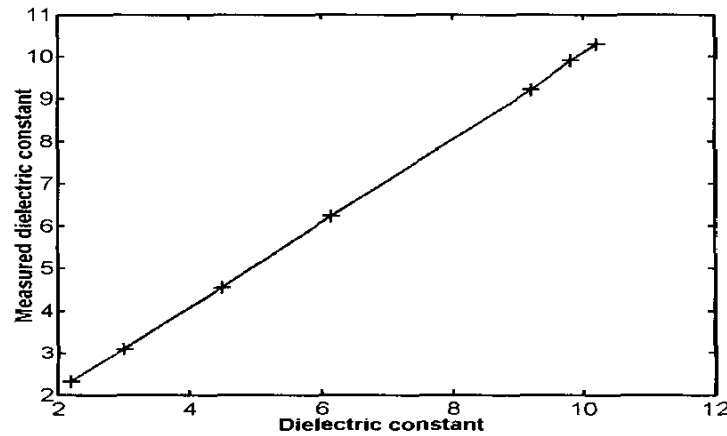


Figure 8 The measured permittivity of samples with known permittivity value. The agreement between the measured and actual values is excellent.

IV. Summary

We developed an efficient semi-closed-form numerical method to calculate the charge distribution of probe tip above stratified dielectric or metallic samples. The experiments showed that the simple $\lambda/2$ microstrip resonator has an excellent capacitance resolution nearing 1.96×10^{-18} F using BiCMOS based measurement system at 1 GHz. The estimated CGP matrix was used to estimate the permittivity of the dielectric samples. Less than 7% error has been achieved using non-contact, high spatial resolution measurement at 1 GHz.

V. Reference

- [1] John P. Casey, and Ranjeev Bansal, "Analysis and optimization of an electrically small receiving antenna." *IEEE Trans. Electromag. Compat.*, vol. 33, pp. 197-204, Aug 1991.
- [2] M. Tabib-Azar, N. Shoemaker, and S. Harris, *Meas. Sci. Technol.* 3, 583 (1993).
- [3] M. Tabib-Azar, D.-P. Su, A. Pohar, S. R. LeClair, and G. Ponchak, '0.4 μm spatial resolution with 1 GHz ($\lambda = 30$ cm) evanescent microwave probe', *Rev. Sci. Instrum.* Vol 70, 1725 (1999).

- [4] Tabib-Azar, M. et al., "Acousto-electromagnetic properties of human dentin." IEEE-EMBS Special Topic Issue on Microtechnologies in Medicine and Biology (Cat. No.02EX578) 2002 p.189-92
- [5] Tabib-Azar, M., Ruoxun Wang, "Planar evanescent microwave imaging probes for nondestructive evaluation of materials with very high spatial resolution and scan rates." Seventh Annual Review of Progress in Quantitative Nondestructive Evaluation, n 557 2001 p.446-53.
- [6] M. Tabib-Azar, J. L. Katz, S. LeClair, "Evanescent Microwaves: A Novel, Super-resolution, Noncontact and Nondestructive Imaging Technique for Biological Applications." IEEE Trans. on Instrumentation and Measurement, pp. 1111-1118 (1999).
- [7] M. Tabib-Azar and S. R. LeClair, "Applications of Evanescent Microwave Probes in Gas and Chemical Sensors." Sensors and Actuators B 67, pp. 112-121 (2000).
- [8] M. Tabib-Azar, R. Ciocan, G. Ponchak and S. R. LeClair, "Transient Thermography Using Microwave Microscope." Review of Scientific Instruments, Vol. 70 (8), pp. 3387-3391 (1999).
- [9] M. Tabib-Azar and B. Sutapun, "Novel Hydrogen Sensors Using Evanescent Microwave Probes." Review of Scientific Instruments, Vol. 70 (9), pp. 3707-3714 (1999).
- [10] M. Tabib-Azar and D. Akinwande, "Real-Time Imaging of Semiconductor Space-Charge Regions Using High-Spatial Resolution Evanescent Microwave Microscope." Rev. of Scientific Instr. Vol. 71 (3), p. 1725-1730 (2000).
- [11] M. Sancho, J. L. Sebastian, S. Munoz, and J. M. Miranda, "Computational method in electrostatics based on Monte Carlo energy minimization." *Proc. IEEE Science, Measurement and Technology*, vol. 148. pp.121-124, May 2001.